Tunable Terahertz Absorber Based on Bulk-Dirac-Semimetal Metasurface

Yannan Jiang
Wan Xinguo
Jiao Wang
Jia Wang

**Ultrathin & Tunable
Terahertz absorber!**
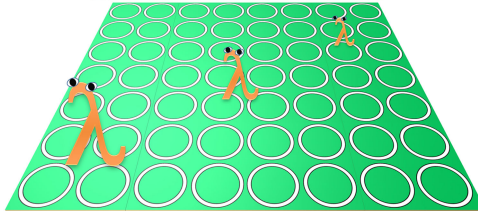
Tunable Terahertz Absorber Based on Bulk-Dirac-Semimetal Metasurface

Yannan Jiang [ORCID],[1] **Wan Xinguo,**[1] **Jiao Wang** [ORCID],[1] **and Jia Wang**[2]

[1]Guangxi Key Laboratory of Wireless Wideband Communication and Signal Processing, Guilin 541004, China
[2]School of Computer Science and Engineering, Southeast University, Nanjing 211189, China

Abstract: We propose a tunable terahertz (THz) absorber design that utilizes a bulk Dirac semimetal (BDS)-based metasurface. The absorber consists of a BDS film with a periodic ring slot, dielectric layer, and fully reflective gold mirror. Simulations indicate that localized surface plasmon resonance is excited within certain regions close to the ring slot, leading to dipolar plasmon resonance of periodic arrays along the polarization direction, thereby producing resonant absorption. The BDS conductivity scales linearly with the Fermi level that can be tuned by bias application, enhancing the electromagnetic-field concentration and shrinking the effective current path, thereby blue-shifting the operating frequency within an ultrawideband. The thickness of the proposed design is significantly less than the resonant wavelength; therefore, the design yields an ultrathin metasurface absorber. This paper may lead to the investigations of the tunable metasurface device based on the BDS.

Index Terms: Absorber, metasurface, bulk Dirac semimetal (BDS).

1. Introduction

Terahertz (THz) technology, which operates in the "terahertz gap" within a frequency range of 0.1 THz – 10 THz, has been found promising for use in myriad applications such as communication, imaging, spectroscopy, and biosensing [1], [2]. Electromagnetic-wave absorbers, which form key components in these applications, have consequently begun attracting increasing attention [3]. Conventional absorbers such as pyramid-based ones [4] suffer from demerits such as bulky configurations and lack of tunability.

Over the past few years, metamaterials have enabled the realization of many phenomena and functionalities unavailable through the use of natural materials [5]. In particular, a type of ultrathin metamaterial, called a metasurface, has attracted tremendous attention in the light of the design functionalities (including absorption) it affords due to its prominent light manipulation abilities, multifunctionality, and ease of on-chip fabrication resulting from its planar structure [6]–[8]. Customarily, metasurfaces have mostly been investigated via patterning noble metals such as silver and gold

in the microwave and terahertz frequency ranges [6]–[11]. Nevertheless, the absence of device tunability still forms a major obstacle to practical application.

Recently, two-dimensional (2D) materials with atomic-scale thicknesses, such as graphene and black phosphorus (BP), have shown extraordinary promise as potential metasurfaces. In particular, graphene is known for its unique electronic and optical properties arising due to the presence of 2D Dirac fermions in its electronic structure [12]–[14], and BP is characterized by its puckered hexagonal honeycomb structure with ridges due to sp^3 hybridization [15]–[18]. Most importantly, these two materials can be regarded as suitable candidates for the design of tunable metasurfaces in terms of the inherent adjustability of their Fermi level (E_F) [19]–[24]. For example, optical polarization encoding to dynamically modulate the polarization state of light over a widely tunable range can be realized with the use of a graphene-loaded metasurface [19], [20]. Graphene-based metasurfaces have been utilized to enhance and tune the plasmonic resonances [21], [22]. In Refs. [23] and [24], tunable absorbers utilizing a BP-based metasurface have been proposed for operation in the infrared regime. However, their moderate carrier mobilities (e.g., 2×10^5 cm^{2}V^{-1}s^{-1} at 5 K for graphene [25] and 5×10^5 cm^{2}V^{-1}s^{-1} at 30 K for BP [26]) are still a limitation to their application.

More recently, bulk Dirac semimetals (BDSs), also called "three-dimensional (3D)-graphene-type" 3D Dirac semimetals, such as Cd$_3$As$_2$, ZrTe$_5$, and AlCuFe, have attracted significant attention due to their ultrahigh mobility of up to 9×10^6 cm^{2}V^{-1}s^{-1} at 5 K [27], [28]. For instance, Chen *et al.* investigated the realization of the tunable plasmon-induced transparency effect at terahertz frequencies in Dirac semimetal metamaterials [29]–[31]. Further, in Ref. [32], a 3D topological Dirac semimetal thin film exhibiting ultrafast nonlinear absorption in the near-infrared band has been reported. However, the potential of the BDSs as regards their application to metasurface-based absorbers has not been exploited thus far.

In this study, we firstly investigate the frequency-dependent conductivity model of a BDS for different E_F values, and subsequently, we propose a tunable metasurface absorber based on the BDS material for operation in the terahertz gap. This absorber consists of a BDS film patterned with a ring slot array, dielectric layer, and fully reflective gold mirror. Within a certain region close to the ring slot, a dipolar plasmon resonance of periodic arrays along the polarization direction is formed, and subsequently, a resonant absorption peak is produced. Furthermore, a higher E_F value corresponds to greater conductivity σ, which can be adjusted by external bias and used to tune the absorptive performance. The fundamental principle underlying the blue shift of the operating frequency with increasing E_F is elaborated. One of most important contributions of the study is the realization of an ultrathin structure with this design; the thickness of the device is less than one-seventeenth the resonant wavelength in the dielectric layer. In addition, the proposed device can operate satisfactorily over a wide incident angle range.

2. Conductivity Model of BDS

In the long-wavelength limit (local response approximation), the longitudinal dynamic conductivity of the Dirac 3D electron gas in the BDSs can be calculated using the Kubo formalism in the random-phase approximation. In the case of electron–hole (e–h) symmetry of the Dirac spectrum for a low-temperature limit such as $T \ll E_F$, the complex conductivity can be approximately expressed as [28]

$$\mathrm{Re}\sigma(\Omega) = \frac{e^2}{\hbar} \frac{gk_F}{24\pi} \Omega\theta(\Omega - 2) \tag{1}$$

$$\mathrm{Im}\sigma(\Omega) = \frac{e^2}{\hbar} \frac{gk_F}{24\pi} \left[\frac{4}{\Omega} - \Omega \ln\left(\frac{4\varepsilon_c}{|\Omega^2 - 4|} \right) \right] \tag{2}$$

Here, e denotes the electron charge, $\hbar$ the reduced Planck constant, g the degeneracy factor, and θ the Riemann–Siegel theta function. The Fermi momentum k_F can be expressed as $E_F/\hbar v_F$ with v_F denoting the Fermi velocity and E_F the Fermi level, in which E_F can be tuned by bias application. The other parameters can be set as $\Omega = \hbar\omega/E_F + jv_F/(E_F k_F \mu)$ with carrier mobility
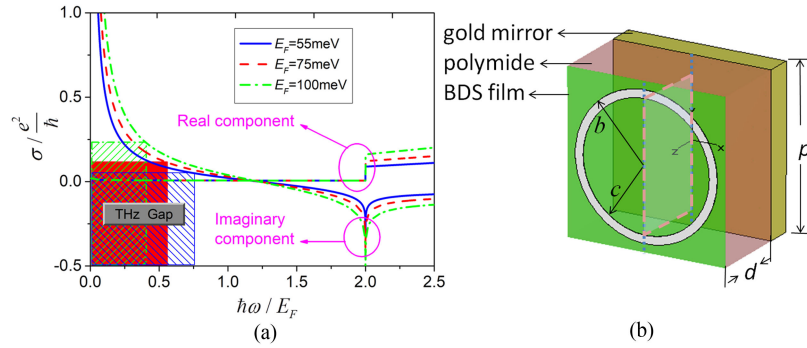
Fig. 1. (a) Normalized frequency ($\hbar\omega/E_F$)-dependent conductivity model of bulk Dirac semimetal (BDS) in unit $e^2/\hbar$ for different E_F values at zero temperature: the parameters of the BDS are set as $g = 40$, $\varepsilon_c = 3$, $v_F = 10^6$ m/s, and $\mu = 3 \times 10^4$ cm^{2}V^{-1}s^{-1}. The normalized frequency ranges covered by the hatched regions are the corresponding terahertz gaps being less than 10 THz, i.e., $\hbar\omega/E_F \cong 0.752$, 0.551, and 0.414 for 10 THz when $E_F = 55$ meV, 75 meV, and 100 meV, respectively. (b) Cell schematic of proposed BDS-based metasurface absorber. The dashed and closed loop is located on the yoz plane.

and $\varepsilon_c = E_c/E_F$ with cutoff energy E_c. In Eq. (2), the first term and the second term derive from the intraband conductivity and the negative contribution of the interband transitions, respectively. In this study, we choose AlCuFe quasicrystals as the BDS metamaterial and plot the dynamic conductivity of the BDS with $g = 40$, $Ec = 3$, $v_F = 10^6$ m/s, and $\mu = 3 \times 10^4$ cm^2 V^{-1}s^{-1}, as shown in Fig. 1(a). The blue (solid), red (dash), and green (dash-dot) lines indicate the conductivity for $E_F = 55$ meV, 75 meV, and 100 meV, respectively. At $\hbar\omega/E_F > 2$, the real component is linear with frequency. It is clear that in the terahertz gap, the imaginary component is far greater than the real component, which can thus be neglected. Moreover, the conductivity increases with E_F, which provides the approach for the design of our tunable BDS-based device.

3. Results and Discussion

The cell schematic of the proposed BDS-based metasurface absorber is shown in Fig. 1(b). The absorber consists of a BDS film with a ring slot, a dielectric layer with permittivity $\varepsilon_r = 3.5$, and a fully reflective gold mirror. In this design, we employ a BDS of thickness 20 nm. In the analysis, periodicity p, polyimide thickness d, outer radius b, and inner radius c are varied; it is evident that $w = b - c$ is the width of the ring slot.

The proposed absorber was investigated via simulations using the Microwaves & RF Optical module in CST Microwave Studio package. To emulate the BDS, we calculated its conductivity by Eqs. (1) and (2) and then import them into the package. In the simulations, periodic boundary conditions were employed along the x– and y–directions to replicate an infinite array of the metasurface while the open boundary conditions were applied along the z-direction. Unless mentioned otherwise, the periodic structure is illuminated by a normal incident plane wave. The absorption can be obtained as $A(f) = 1 - R(f) - T(f)$ with reflection given by $R(f) = |S_{11}(f)|^2$ and transmission given by $T(f) = |S_{21}(f)|^2$, where f denotes the frequency, and $S_{11}(f)$ and $S_{21}(f)$ denote the frequency-dependent S-parameters. Because of the presence of the fully reflective gold mirror and the consequent prevention of wave propagation, transmission is regarded as zero over the entire frequency range investigated. Therefore, $A(f) = 1 - R(f)$.

In the first simulation, the Fermi level E_F of the BDS was set to be 75 meV, and the other geometrical parameters were set as $p = 6$ μm, $b = 2.7$ μm, and $w = 0.3$ μm. The simulated absorptions of the proposed absorber for different d values are shown in Fig. 2(a). We note that the peak absorption intensity first increases and then decreases with increase in d. Moreover, the absorption is greater than 90% when $d = 2$ μm and 3 μm. Next, given a fixed $d = 3$ μm, absorption was realized by changing p from 6 μm to 16 μm in increments of 2 μm while maintaining the
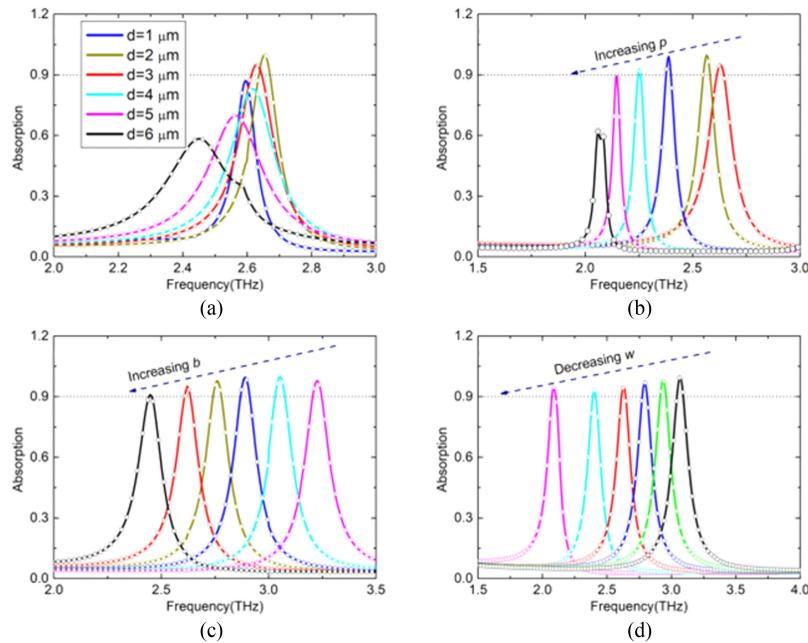
Fig. 2. Simulated absorptions for (a) different d values, (b) p increasing from 6 μm to 16 μm in increments of 2 μm, (c) b increasing from 1.9 μm to 2.9 μm in increments of 0.2 μm, and (d) w decreasing from 0.6 μm to 0.1 μm in decrements of 0.1 μm. The open circles and solid lines indicate the absorptions for transverse magnetic (TM) polarization and transverse electric (TE) polarization, respectively.

other parameters constant, as shown in Fig. 2(b). For $p < 14$ μm, the peak absorption intensities are greater than 90%. It can also be observed that the absorption peak exhibits a red shift with increasing p. Next, we investigated the performance of the BDS-based absorber by modifying the outer radius b from 1.9 μm to 2.9 μm when $p = 6$ μm, as shown in Fig. 2(c). It is obvious that the absorption peak exhibits a red shift with increasing b, and the resonant depth value increases slightly and then decreases. It is interesting that the resonant wavelength λ_e for different b values is proportional to the length $a = 2(2c + d)$, which is approximately equal to the perimeter of the effective current path, as indicated by the dashed and closed loop in Fig. 1(b), and the relationship of $a \approx \lambda_e/4$ holds, as indicated by the black solid line with open circles in Fig. 3, where λ_e represents the resonant wavelength $\lambda_e = \lambda/\sqrt{\varepsilon_r}$ with wavelength λ in free space. A similar phenomenon is also observed when p is varied (see the dashed line with filled circles in Fig. 3).

In order to understand the physical mechanism underlying the absorption, we plotted the electric field distributions and surface current distributions on the surface of the BDS material for TE polarization (insets of Fig. 3). In these insets, the electric field mainly concentrates within the certain regions close to the upper and lower halves of the ring slot (see (a), (b) and (c)), and the current intensity inside the ring is dominant (see (d), (e) and (f)). Therefore, a dipolar plasmon resonance of periodic arrays along the y-direction is formed by the electric field concentrating along both half-ring slots. Hence, increments in p and b can "stretch" the effective current path, which can lead to increment in the resonant wavelength and decrement in the resonant frequency. Similarly, given fixed p and b values, a decrease in w leads to increase in a, and we can subsequently predict that the resonant wavelength will increase with red-shift of the absorption peak, as shown in Fig. 2(d).

Figs. 2(a), (b), (c), and (d) depict the absorptive performances for TE and TM waves, as indicated by the open circles and solid lines, respectively. A close consistency is observed between both cases due to the existence of the fourfold rotational symmetry in the cell structure about the z-axis, which indicates that the proposed absorber is independent of the polarization of the incident wave.
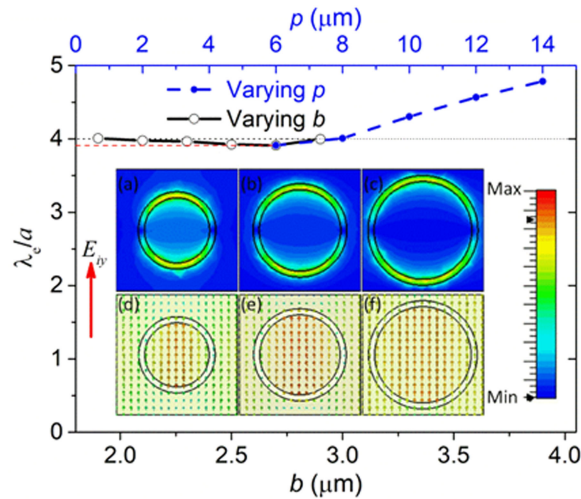
Fig. 3. Ratios of resonant wavelength λ_e and a for ring slot for different b values when $p = 6$ μm (black solid line with open circles) and for different p values when $b = 2.7$ μm (blue dashed line with filled circles). The insets show the electric field distributions [(a), (b), and (c)] and the surface current distributions [(d), (e), and (f)] at 3.24 THz, 2.94 THz, and 2.63 THz for $b = 1.9$ μm, 2.3 μm, and 2.7 μm, respectively, when $p = 6$ μm and the incident wave is a transverse electric (TE) wave.
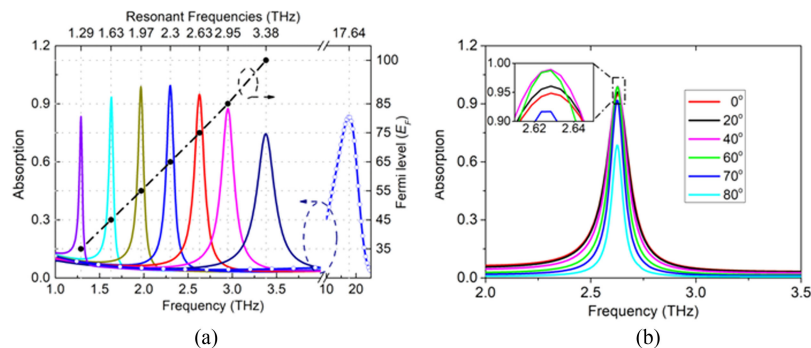

Fig. 4. (a) Frequency-dependent absorption of proposed absorber based on bulk Dirac semimetal (BDS) with different Fermi levels (solid lines) and of absorber with BDS being replaced by gold (solid line with open circles) excited by normal incident wave: the dashed line with filled circles indicates the approximate linear relationship between resonant frequencies and the Fermi level; the frequencies at the data points corresponding to the filled circles are 1.29 THz, 1.63 THz, 1.97 THz, 2.3 THz, 2.63 THz, 2.95 THz, and 3.38 THz when $E_F = 35$ meV, 45 meV, 55 meV, 65 meV, 75 meV, 85 meV, and 100 meV, respectively. (b) Frequency-dependent absorption of proposed absorber excited by plane wave at different incident angles for BDS with $E_F = 75$ meV.

As shown in Fig. 1(a), the conductivity varies with change in E_F (the higher is E_F, the greater is σ), which can be controlled by bias application and chemical doping. Therefore, the reconfigurable absorptive performance of the proposed BDS absorber can also be predicted. In our study, parameters p, d, b, and c were set to be 6 μm, 3 μm, 2.7 μm, and 2.4 μm, respectively. The absorption spectra for different E_F values are shown in Fig. 4(a). Obviously, the absorption peak shows a blue shift with increasing E_F (colorful solid lines), and the proposed BDS-based absorber can operate dynamically in the frequency range of $\sim$1.5 THz and $\sim$2.75 THz with the absorption being greater than 90%, i.e., the relative bandwidth is about 58.8%. Here, it is interesting to note that the resonant frequencies are approximately linearly dependent on E_F, as indicated by the dash-dotted line with filled circles.
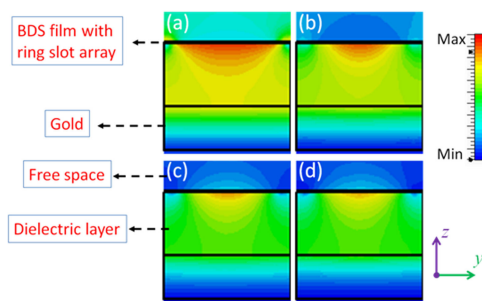
Fig. 5. Magnetic amplitude distributions across the yoz section at resonant frequencies when (a) $E_F = 35$ meV, (b) $E_F = 55$ meV, (c) $E_F = 75$ meV, and (d) $E_F = 100$ meV.

To understand the physical principles underlying this blue shift of the absorption peak with increase in E_F, we study the magnetic field distributions across the yoz section (see the dashed and closed plane in Fig. 1(b)) at the respective resonant frequencies corresponding to $E_F = 35$ meV, 55 meV, 75 meV, and 100 meV, as shown in Figs. 5 (a), (b), (c), and (d), respectively. From Fig. 1(a) and Eqs. (1) and (2), we note that an increment in E_F will lead to increase in the conductivity and enhance the conductive performance of the BDS, which will subsequently enhance the concentration of the electromagnetic field and shrink the effective current path between the gold mirror and BDS film (obviously, the field appears more and more concentrated from Fig. 5(a) to Fig. 5 (d)), which then leads to the blue shift.

Moreover, from Figs. 2 (c), (d), and Fig. 4, we can infer that thickness d of the BDS-based absorber lies in the range of $\lambda_e/26$ and $\lambda_e/17$. This indicates that an ultrathin design of the proposed BDS-based absorber is possible. Meanwhile, when the BDS is replaced by gold, the corresponding absorption curve is indicated by the solid line with open circles in Fig. 4(a). In this case, the resonant frequency is 17.64 THz, with thickness d being only about $\lambda_e/3$. This result indicates the BDS plays a significant role in the realization of the metasurface design.

In order to demonstrate the absorptive performance, we next excited the proposed device with a plane wave at different incident angles (i.e., the angle between the z-axis and wave vector **K** in the xoz plane). The absorptions for incident angles varying from 0° to 90° are shown in Fig. 4(b). It is obvious that the absorption is greater than 90% when the incident angle is less than 70°. Moreover, the operating frequency remains unchanged. This result indicates that the proposed BDS-based metasurface absorber can exhibit good stability over a wide incident angle range.

4. Conclusion

In conclusion, we proposed the theoretical model of a tunable metasurface absorber based on a BDS material in the THz regime. The model is formed by a BDS film with a ring slot array, dielectric layer, and fully reflective gold mirror. Both the absorption performance and the physical mechanism of absorption were investigated. Our results indicate that an absorption peak of greater than 90% can be tuned with a relative bandwidth of 58.8% in the terahertz gap. The thickness of the introduced absorber model varies from $\lambda_e/26$ to $\lambda_e/17$, which indicates that the use of the BDS can lead to a compact device design when compared with a noble-metal-based device. Our findings can contribute to the development of applications such as terahertz detectors, thermal emitters, and imaging.

References

[1] B. Sensale-Rodriguez *et al.*, "Broadband graphene terahertz modulators enabled by intraband transitions," *Nature Commun.*, vol. 3, no. 1, 2012, Art. no. 780.
[2] Y. J. Guo, K. D. Xu, and X. Tang, "Spoof plasmonic waveguide developed from coplanar stripline for strongly confined terahertz propagation and its application in microwave filters," *Opt. Exp.*, vol. 26, no. 8, pp. 10589–10598, 2018.

[3] C. M. Watts, X. Liu, and W. J. Padilla, "Metamaterial electromagnetic wave absorbers," *Adv. Mater.*, vol. 24, no. 23, pp. 98–120, 2012.

[4] S. P. Lv, S. H. Liu, and Y. B. Zhao, "Design and analysis of a pyramid absorber vertex angle," *Mater. Technol.*, vol. 20, no. 4, pp. 211–213, 2005.

[5] N. K. Grady *et al.*, "Terahertz metamaterials for linear polarization conversion and anomalous refraction," *Science*, vol. 340, pp. 1304–1307, 2013.

[6] J. Wang and Y. Jiang, "Gradient metasurface for four-direction anomalous reflection in terahertz," *Opt. Commun.*, vol. 416, pp. 125–129, 2018.

[7] H. X. Xu, S. Tang, X. Ling, W. Luo, and L. Zhou, "Flexible control of highly-directive emissions based on bifunctional metasurfaces with low polarization cross-talking," *Ann. Phys. (Berlin)*, vol. 529, no. 5, 2017, Art. no. 1700045.

[8] H. X. Xu *et al.*, "Deterministic approach to achieve broadband polarization-independent diffusive scatterings based on metasurfaces," *ACS Photon.*, vol. 5, no. 5, pp. 1691–1702, 2018.

[9] H. X. Xu, G. M. Wang, M. Q. Qi, J. G. Liang, J. Q. Gong, and Z. M. Xu, "Triple-band polarization-insensitive wide-angle ultra-miniature metamaterial transmission line absorber," *Phys. Rev. B*, vol. 86, no. 20, 2012, Art. no. 205104.

[10] Y. J. Guo, K. D. Xu, Y. Liu, and X. Tang, "Novel surface plasmon polariton waveguides with enhanced field confinement for microwave-frequency ultra-wideband bandpass filters," *IEEE Access*, vol. 6, pp. 10249–10256, 2018.

[11] Y. Jiang, L. Wang, J. Wang, C. N. Akwuruoha, and W. Cao, "Ultra-wideband high-efficiency reflective linear-to-circular polarization converter based on metasurface at terahertz frequencies," *Opt. Exp.*, vol. 25, no. 22, pp. 27616–27623, 2017.

[12] J. Wang, C. N. Gao, Y. Jiang, and C. N. Akwuruoha, "Ultra-broadband and polarization-independent planar absorber based on multilayered graphene," *Chin. Phys. B*, vol. 26, no. 11, 2017, Art. no. 114102.

[13] X. Huang *et al.*, "Binder-free highly conductive graphene laminate for low cost printed radio frequency applications," *Appl. Phys. Lett.*, vol. 106, no. 20, 2015, Art. no. 203105.

[14] X. Huang, T. Leng, K. H. Chang, J. C. Chen, K. S. Novoselov, and, Z. Hu, "Graphene radio frequency and microwave passive components for low cost wearable electronics," *2D Mater.*, vol. 3, no. 2, 2016, Art. no. 025021.

[15] S. C. Dhanabalan, J. S. Ponraj, Z. Guo, S. Li, Q. Bao, and H. Zhang, "Emerging trends in phosphorene fabrication towards next generation devices," *Adv. Sci.*, vol. 4, no. 6, 2017, Art. no. 1600305.

[16] J. D. Shao *et al.*, "Biodegradable black phosphorus-based nanospheres for in vivo photothermal cancer therapy," *Nature Commun.*, vol. 7, 2016, Art. no. 12967.

[17] W. Tao *et al.*, "Black phosphorus nanosheets as a robust delivery platform for cancer theranostics," *Adv. Mater.*, vol. 29, no. 1, 2017, Art. no. 1603276.

[18] Q. Q. Jiang, L. Xu, N. Chen, H. Zhang, L. M. Dai, and S. Y. Wang, "Facile synthesis of black phosphorus: An efficient electrocatalyst for the oxygen evolving reaction," *Angewandte Chemie*, vol. 55, no. 44, pp. 13849–13853, 2016.

[19] J. Li *et al.*, "Polarization: Optical polarization encoding using graphene-loaded plasmonic metasurfaces," *Adv. Opt. Mater.*, vol. 4, no. 1, pp. 91–98, 2016.

[20] Y. Fan *et al.*, "Electrically tunable Goos–Hänchen effect with graphene in the terahertz regime," *Adv. Opt. Mater.*, vol. 4, no. 11, pp. 1824–1828, 2016.

[21] Y. Fan, N. H. Shen, T. Koschny, and C. M. Soukoulis, "Tunable terahertz meta-surface with graphene cut-wires," *ACS Photon.*, vol. 2, no. 1, pp. 151–156, 2014.

[22] Y. Fan *et al.*, "Photoexcited graphene metasurfaces: Significantly enhanced and tunable magnetic resonances," *ACS Photon.*, vol. 5, no. 4, pp. 1612–1618, 2018.

[23] J. Wang and Y. Jiang, "Infrared absorber based on sandwiched two-dimensional black phosphorus metamaterials," *Opt. Exp.*, vol. 25, no. 5, pp. 5206–5216, 2017.

[24] J. Wang, Y. Jiang, and Z. Hu, "Dual-band and polarization-independent infrared absorber based on two-dimensional black phosphorus metamaterials," *Opt. Exp.*, vol. 25, no. 18, pp. 22149–22157, 2017.

[25] K. I. Bolotin *et al.*, "Ultrahigh electron mobility in suspended graphene," *Solid State Commun.*, vol. 146, no. 9, pp. 351–355, 2008.

[26] F. Xia, H. Wang, D. Xiao, M. Dubey, and A. Ramasubramaniam, "Two-dimensional material nanophotonics," *Nature Photon.*, vol. 8, no.12, pp. 899–907, 2015.

[27] T. Liang, Q. Gibson, M. N. Ali, M. Liu, R. J. cava, and N. P. Ong, "Ultrahigh mobility and giant magneto resistance in the Dirac semimetal Cd3As2," *Nature Mater.*, vol. 14, pp. 280–284, 2015.

[28] O. V. Kotov and Y. E. Lozovik, "Dielectric response and novel electromagnetic modes in three-dimensional Dirac semimetal films," *Phys. Rev. B*, vol. 93, no. 23, 2016, Art. no. 235417.

[29] H. Chen, H. Zhang, M. Liu, Y. Zhao, X. Guo, and Y. Zhang, "Realization of tunable plasmon-induced transparency by bright-bright mode coupling in Dirac semimetals," *Opt. Mater. Exp.*, vol. 7, no. 9, pp. 3397–3407, 2017.

[30] H. Chen, H. Zhang, X. Guo, S. Liu, and Y. Zhang, "Tunable plasmon-induced transparency in H-shaped Dirac semimetal metamaterial," *Appl. Opt.*, vol. 57, no. 4, pp. 752–756, 2018.

[31] H. Chen, H. Zhang, Y. Zhao, S. Liu, M. Cao, and Y. Zhang, "Broadband tunable terahertz plasmon-induced transparency in Dirac semimetals," *Opt. Laser Technol.*, vol. 104, pp. 210–215, 2018.

[32] Y. Meng *et al.*, "Three-dimensional Dirac semimetal thin-film absorber for broadband pulse generation in the near-infrared," *Opt. Lett.*, vol. 43, no. 7, pp. 1503–1506, 2018.